Article

Possible Evidence for Berezinskii–Kosterlitz–Thouless Transition in Ba(Fe$_{0.914}$Co$_{0.086}$)$_2$As$_2$ Crystals

Wen-He Jiao [1,2,*](ID), Xiao-Feng Xu [3](ID), Hao Jiang [4], Zhu-An Xu [1], Qing-Hu Chen [1] and Guang-Han Cao [1,*]

1   Interdisciplinary Center for Quantum Information, Zhejiang Province Key Laboratory of Quantum Technology and Devices, Department of Physics, Zhejiang University, Hangzhou 310027, China; zhuan@zju.edu.cn (Z.-A.X.); qhchen@zju.edu.cn (Q.-H.C.)
2   Ningbo Institute of Materials Technology and Engineering, Chinese Academy of Sciences, Ningbo 315201, China
3   Department of Applied Physics, Zhejiang University of Technology, Hangzhou 310023, China; xuxiaofeng@zjut.edu.cn
4   School of Physics and Optoelectronics, Xiangtan University, Xiangtan 411105, China; jialay@zju.edu.cn
*   Correspondence: whjiao@nimte.ac.cn (W.-H.J.); ghcao@zju.edu.cn (G.-H.C.)

Abstract: In this study, we measure the in-plane transport properties of high-quality Ba(Fe$_{0.914}$Co$_{0.086}$)$_2$As$_2$ single crystals. Signatures of vortex unbinding Berezinskii–Kosterlitz–Thouless (BKT) transition are shown from both the conventional approach and the Fisher–Fisher–Huse dynamic scaling analysis, in which a characteristic Nelson–Kosterlitz jump is demonstrated. We also observe a non-Hall transverse signal exactly at the superconducting transition, which is explained in terms of guided motion of unbound vortices.

Keywords: Berezinskii–Kosterlitz–Thouless transition; superconducting transition; vortices

1. Introduction

Uncovering the underlying essential universality for high-temperature superconductivity is extremely important for understanding the superconducting mechanism as well as exploring the next high-T_c materials [1]. The two classes of high-temperature superconductors discovered, Cu-based superconductors (CuSCs) and Fe-based superconductors (FeSCs), bear many similarities, regardless of some differences [1–3]. Apparently, FeSCs contain two-dimensional (2D) FeAs layers, analogous to the 2D CuO$_2$ planes in CuSCs. More similarities were manifested by the antiferromagnetism in parent compounds, superconducting phase diagrams with respect to chemical doping, and extreme type-II superconductivity with very high upper critical field, etc. However, FeSCs show unusually small anisotropy in the upper critical field [4,5], which is in sharp contrast with CuSCs [6]. So far, there is no consensus on the nature of dimensionality in FeSCs [1], unlike the situation in CuSCs where the 2D characteristic is widely observed, [6] and the 2D nature is considered to be crucial for high-T_c superconductivity [7].

Quasi-2D superconducting behaviors in CuSCs are demonstrated by a 2D Berezinskii–Kosterlitz–Thouless (BKT) topological phase transition [8] close to the mean-field superconducting transition temperature (T_c^{MF}), even for the bulk crystals [9–13]. Such a novel BKT-type transition was earlier discussed in terms of vortex–antivortex dissociation in an ideal 2D superconductor [14], and then it was experimentally observed in ultra-thin superconducting films [15]. For CuSCs, because of the negligibly weak interlayer superconducting coupling near T_c^{MF}, vortex fluctuations [16], or thermal distortions [17] in Josephson coupled layered materials, 2D BKT behavior was able to be observed in bulk crystals of Bi$_2$Sr$_2$CaCu$_2$O$_8$ [9,10], YBa$_2$Cu$_3$O$_7$ [11,12], and La$_{1.875}$Ba$_{0.125}$CuO$_4$ [13]. The expected unbound free vortices near the superconducting transition are independently supported by the observation of non-zero transverse voltage at zero field (hereafter denoted as V_0^{xy}) [18,19]. The 2D superconducting phase fluctuations are also evidenced

even well above the superconducting transition temperature [20], shedding light on the superconducting mechanism of CuSCs.

As for FeSCs, either 2D or 3D of the nature of superconducting fluctuations is reported [21–26], and an apparent contradiction appeared in a few cases. For example, 2D nature of superconductivity was implied by the study of fluctuation conductivity in F-doped SmFeAsO polycrystals [21] and single crystals [22], while fluctuations in $SmFeAsO_{0.8}F_{0.2}$ was reported to have a 3D character and extend far above T_c [24]. Recently, the evidence of BKT transition was reported in $FeTe_{0.55}Se_{0.45}$ thin films, suggesting a quasi-2D characteristic in such systems [27]. This finding motivates us to explore possible BKT transition in other FeSCs. In this study, we report possible evidence for BKT phase transition in a typical FeSC, $Ba(Fe_{1-x}Co_x)_2As_2$ [28] with $x = 0.086$, via both the conventional approach and the Fisher–Fisher–Huse (FFH) [29] dynamic scaling analysis. The characteristic Nelson–Kosterlitz jump for a BKT transition is demonstrated. In addition, we observe non-Hall-type transverse signal including V_0^{xy}, exactly above the possible BKT transition temperature T_{BKT}, pointing to the existence of thermally excited unbound vortices.

2. Experimental Methods

The $Ba(Fe_{0.914}Co_{0.086})_2As_2$ crystals were grown by a self-flux method with procedures similar to Ref. [30]. The chemical composition of the crystal was determined by an energy-dispersive x-ray spectroscope affiliated to a field-emission scanning electron microscope (FEI Model SIRION), giving the title chemical formula (the Co-content uncertainty was ± 0.005). The T_c^{onset} temperature-dependent in-plane resistance shows a sharp superconducting transition at $T_c^{onset} = 25.0$ K, as seen in the inset of Figure 1. The transition width $[\Delta T_c = T(90\%\rho_n) - T(10\%\rho_n)$, where ρ_n is the normal-state resistivity at $T_c^{onset}]$ is as narrow as 0.42 K, indicating high quality with good homogeneity for the crystal. The relatively high T_c value indicates that the crystal was in the optimally-doped regime, consistent with the cobalt content measured.
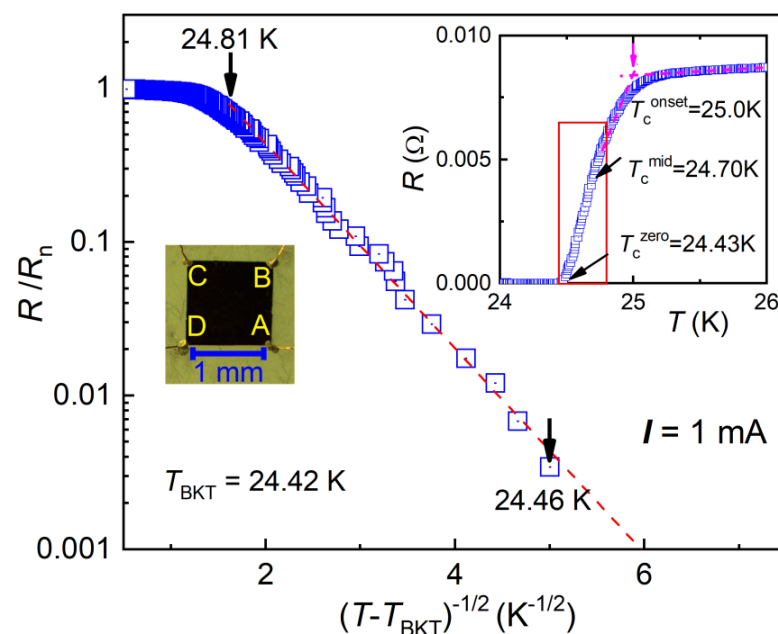
Figure 1. Temperature dependence of normalized resistance R/R_n in the superconducting transition of $Ba(Fe_{0.914}Co_{0.086})_2As_2$ crystal (photographed on the left inset). Rn is the normal-state resistance, obtained by a linear extrapolation from 50 K to 35 K. The inserted plot shows the superconducting transition in normal linear scale. The related characteristic temperatures are indicated with arrows.

The electro-transport measurements were performed on a Quantum Design Physical Property Measurement System (PPMS-9). We adopted a van der Pauw four-terminal

configuration [31] for all the measurements, including longitudinal $I - V$ curves and transverse voltages. The crystal was carefully cleaved and cut into a squared specimen with a side length of $L = 1.14$ mm and thickness of $t = 0.024$ mm. Gold wires were attached with silver paste onto the four corners (A, B, C, and D), as shown in the left inset of Figure 1. The longitudinal resistance was obtained by $R_{xx} = (R_{DC/AB} + R_{BC/AD})/2$, where $R_{DC/AB}$ ($R_{BC/AD}$) equals to the potential V_{DC} (V_{BC}) divided by the current I_{AB} (I_{AD}) using ac transport option with a frequency of 13 Hz. The normal-state resistivity above T_c was $\rho_n = \pi t R_{xx}/\ln 2 \sim 0.09$ mΩ cm, consistent with the previous report [28]. The data of $I - V_{xx}$ characteristic were collected at a fixed temperature whose fluctuation was less than 1 mK, without any detectable heating effect during the measurement.

For the measurement of transverse voltage V_{xy}, $V_{BD/AC}$ and $V_{AC/BD}$ were measured respectively by permutating the voltage and current electrodes [32], so that the longitudinal component due to misalignment of the diagonal electrodes can be canceled out. At zero field, one obtains V_{xy}^0 by Ref. [32], $V_{xy}^0 = (V_{BD/AC} - V_{AC/BD})/2$. Obviously, V_{xy}^0 has nothing to do with Hall effect because no magnetic field is applied. It is a non-Hall-type transverse voltage. Under external magnetic fields, similarly, we have two "branches" of the transverse voltage with the field up ($H+$) and down ($H-$), respectively, $V_{xy}^{H+} = (V_{BD;AC}^{H+} - V_{AC;BD}^{H+})/2; V_{xy}^{H-} = (V_{BD;AC}^{H-} - V_{AC;BD}^{H-})/2$. In most cases, V_{xy}^{H+} and V_{xy}^{H-} are mutually antisymmetric, and the conventional Hall voltage can be obtained by $V_{xy}^{Hall} = (V_{xy}^{H+} - V_{xy}^{H-})/2$. When the antisymmetry is broken for some reason, a non-Hall transverse signal V_{xy}^{nH} can be extracted by canceling out the external field effect, $V_{xy}^{nH} = (V_{xy}^{H+} + V_{xy}^{H-})/2$.

3. Data Analysis

To study BKT dynamics in superconductors, there are two main approaches, the "conventional" approach and the dynamic scaling analysis [33]. In the conventional approach, the following signatures in transport properties in the $I \to 0$ A limit are often used to recognize a BKT transition. (1) Within a temperature region slightly above T_{BKT}, the Ohmic longitudinal resistance has a unique temperature dependence [34],

$$R_{xx}(T)/R_n \propto \exp\left\{-2[b(T_c^{MF} - T_{BKT})/(T - T_{BKT})]^{1/2}\right\} \tag{1}$$

where R_n is the normal-state resistance and b is a dimensionless parameter. The mean-field superconducting transition temperature T_c^{MF} is generally set to the midpoint temperature T_c^{mid} (close to the inflection temperature) [9,12,14], which is about 24.70 K. The above exponential behavior is in contrast to that of the paraconductivity effect (due to amplitude fluctuations), which shows a power-law divergence [35]. (2) The isothermal current-voltage relation around T_{BKT} obeys a power law $V \propto I^\alpha$ at low currents, which differs from the exponential dependence for vortex motion, owing to flux depinning [36]. (3) The exponent $\alpha(T)$ has a "universal jump" from 1 to 3 upon approaching T_{BKT} from above. Such a universal jump is regarded as the hallmark of BKT transition. In the BKT theory, $\alpha(T)$ is proportional to the superfluid density, therefore, the jump in $\alpha(T)$ means discontinuity in superfluid density [37], which is called the Nelson–Kosterlitz jump in literature.

According to Equation (1), R/R_n in logarithmic scale is plotted as a function of $(T - T_{BKT})^{-1/2}$ in Figure 1. A linear dependence is shown in between T_c^{zero} and 24.81 K with the fitted parameters $T_{BKT} = 24.42 \pm 0.01$K and $b = 2.10 \pm 0.01$. Note that the T_{BKT} is very close to the zero-resistance temperature T_c^{zero}, similar to previous reports in cuprate systems [9–12]. For $T_c^{mid} < T < T_c^{onset}$, however, paraconductivity effect usually becomes dominant. However, we were not able to fit the $R(T)$ data in this region to either 2D or 3D forms of Aslamazov–Larkin theory [35]. This suggests a dimensional crossover and/or robustness of phase fluctuations in the range of $T_c^{mid} < T < T_c^{onset}$.

The isothermal $I - V$ characteristics at $T = 24.40–24.72$ K with $I = 0.03–4$ mA are displayed in a log–log plot shown in Figure 2a. The linearity confirms the expected power–

law relation. The exponent α, represented by the slope, changes with temperature. For $T > 24.56$ K, the α value is close to 1.0, namely, the $I - V$ curves are basically Ohmic. When approaching T_{BKT}, α increases abruptly, and it goes to 3.6 ± 0.3 at 24.40 K. The inset of Figure 2a clearly shows a jump with $\alpha = 3.0 \pm 0.2$ at T_{BKT}, which suggests the characteristic Nelson–Kosterlitz jump anticipated for a BKT transition.
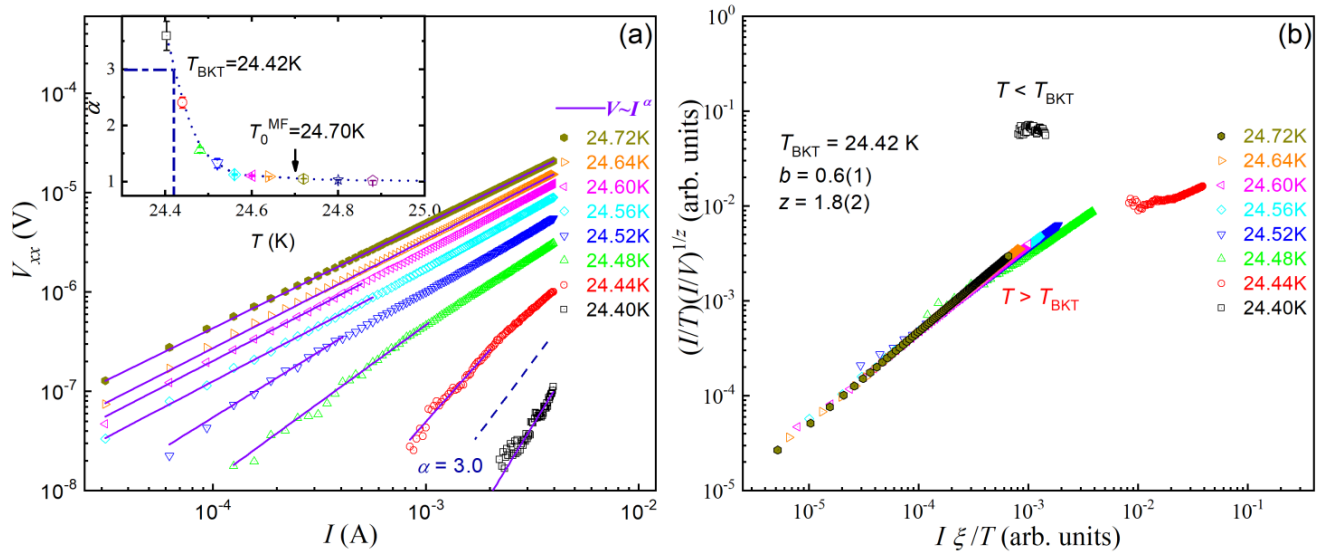
Figure 2. (**a**) A log–log plot of voltage-current characteristics of Ba(Fe$_{0.914}$Co$_{0.086}$)$_2$As$_2$ crystal at temperatures spanning the critical region from 24.40 K to 24.72 K. The inset shows temperature dependence of fitted by $V \propto I^\alpha$ with the low-current data. (**b**) Dynamic scaling of all the $I - V$ data in (**a**) according to Equation (2) in the text.

Strictly speaking, the above approach is valid only in the limit $I \to 0$ A. Thus it is necessary to perform a dynamic scaling analysis, which also holds for finite currents [33]. According to the FFH theory [29], the scaling form for a 2D superconductor can be written as [33,38],

$$(I/T)(I/V)^{1/z} = P_\pm(I\xi_\pm/T) \tag{2}$$

where z is the dynamic exponent, $P_{+(-)}$ is the scaling function for temperature above (below) T_{BKT}, and $\xi_+ \sim \exp[b(T_c^{MF} - T)/(T - T_{BKT})]^{1/2}$ ($\xi_- \sim \exp[b(T_c^{MF} - T_{BKT})/2\pi\left(T_{BKT} - T\right)]^{1/2}$) is the correlation length above (below) T_{BKT}.

Figure 2b plots $I\xi/T$ vs. $(I/T)(I/V)^{1/z}$, according to Equation (2). By setting the afore-determined $T_{BKT} = 24.42$ K, and with the fitted parameters $b = 2.1 \pm 0.1$ and $z = 1.8 \pm 0.2$, all the $I - V$ data points in Figure 2a basically fall onto two branches of the scaling curves (although the branch for $T < T_{BKT}$ are limited to one set of $I - V$ data with $T = 24.40$ K). Since the critical $I - V$ curve follows $V \propto I^{z+1}$ at T_{BKT}, the exponent is 2.8 ± 0.2 at the BKT transition, consistent with the result of above conventional approach. Besides, the value of parameter b is the same with that extracted by fitting R/R_n with Equation (1). Therefore, the FFH dynamic scaling analysis also suggests a BKT phase transition in Ba(Fe$_{0.914}$Co$_{0.086}$)$_2$As$_2$ crystals.

As we know, BKT transition is driven by the unbinding of vortex–antivortex pairs. Below T_{BKT}, the thermally exited vortices are in pairs because of the attractive interaction. At T_{BKT}, the vortex pairs start to unbind, and free vortices are generated due to the contribution of entropy to the free energy. It is the unbound free vortices that contribute to the nonzero longitudinal resistance expressed by Equation (1). Interestingly, such free vortices are able to induce an abnormal nonzero V_{xy}^0, like the case in CuSCs [18,19]. So probing V_{xy}^0 may supply further evidence for the BKT transition.

Figure 3 shows V_{xy}^0 as a function of temperature in Ba(Fe$_{0.914}$Co$_{0.086}$)$_2$As$_2$ crystals. The V_{xy}^0 value is virtually zero in the normal state ($T > T_c^{onset}$) and the superconducting state

($T < T_c^{\text{zero}}$). A nonzero peak-like V_{xy}^0 appears exactly within the region of superconducting transition. The maximum of V_{xy}^0 is located around the midpoint of the resistive transition. It is noted that the sign and the value of the maximal V_{xy}^0 depends on the electrode configuration with respect to the sample orientations. For instance, when the sample is turned over, V_{xy}^0 just changes the sign. Another feature of the nonzero V_{xy}^0 is that the left side of the V_{xy}^0 peak coincides well with the longitudinal signal, i.e., V_{xy}^0 is basically proportional to V_{xx} for $T_c^{\text{zero}} < T < T_c^{\text{mid}}$.
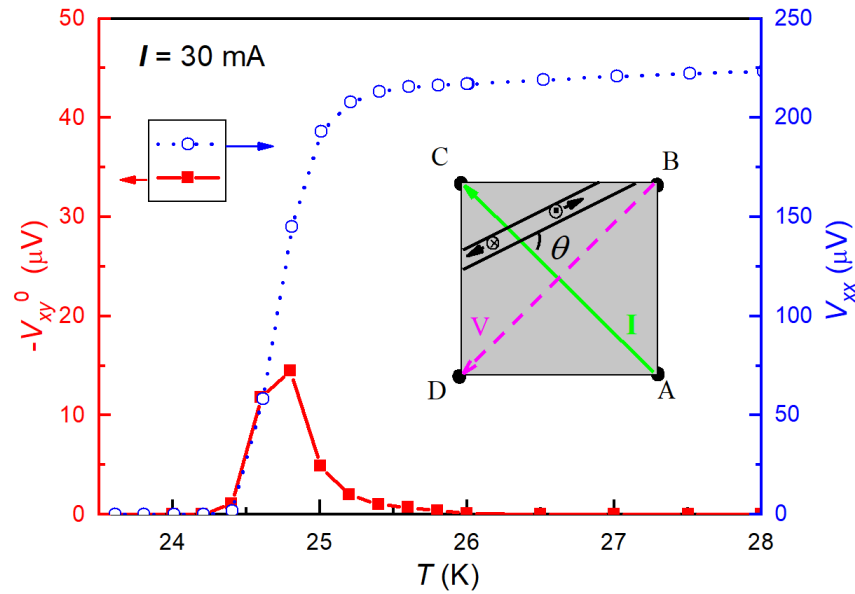
Figure 3. Temperature dependence of the zero-field transverse (left axis) and longitudinal (right axis) voltages for Ba(Fe$_{0.914}$Co$_{0.086}$)$_2$As$_2$ crystals. The transverse voltage was obtained by $V_{xy}^0 = (V_{\text{BD/AC}} - V_{\text{AC/BD}})/2$, and the inset depicts the guided motion of an unbound vortex pair as well as the configuration for the measurement of $V_{\text{BD/AC}}$.

The non-Hall-type transverse voltage in the absence of external magnetic field at superconducting transition was explained by the guided motion of thermally excited vortices [18,19,39]. In Ba(Fe$_{1-x}$Co$_x$)$_2$As$_2$, the guided motion of vortices (or in other words, with anisotropic flux pinning) are supported by the in-plane anisotropy [40] and stripe-like STM image [41]. Assuming a simple situation that fluxons can only move along the guiding direction in an angle θ with respect to the current A $\to$ C as shown in the inset of Figure 3, according to Reference [42], the fully guided motion of vortices generates not only longitudinal electric field,

$$E_{//}^{AC} = n_f \Phi_0 (F_L \sin^2 \theta - F_p \sin \theta)/\eta c \tag{3}$$

but transverse electric field also,

$$E_{\perp}^{BD} = n_f \Phi_0 (F_L \sin \theta \cos \theta - F_p \cos \theta)/\eta c \tag{4}$$

where n_f refers to sheet density of free vortices, Φ_0 is flux quantum, F_p is the weak pinning force along the guiding direction, η is the damping coefficient of vortex motion, and c is the speed of light. When permutating the voltage and current, the angle between the guided motion and current turns out to be $(\pi/2 + \theta)$, and the transverse field due to current B $\to$ D becomes,

$$E_{\perp}^{AC} = n_f \Phi_0 (F_L \sin \theta \cos \theta - F_p \sin \theta)/\eta c \tag{5}$$

Since $V = Ed$ (d is the length of the diagonal of the sample), and $V_{xy}^0 = (V_{BD/AC} - V_{AC/BD})/2$, V_{xy}^0 measured should be,

$$V_{xy}^0 = \sqrt{2} d n_f \Phi_0 F_p \sin(\theta - \pi/4)/\eta c \tag{6}$$

Obviously, V_{xy}^0 is nonzero as long as $\theta \neq (k+1/4)\pi$ (k is an integer) in the presence of free vortices. The sinusoidal variation on θ qualitatively agrees with our experimental observation that V_{xy}^0 depends on the electrode configuration with respect to the sample orientations. When the sample is turned over, and the same electrode configuration is kept, θ changes into $(\pi/2 - \theta)$. Equation (6) gives $V_{xy}^0\big|_{\theta \to (\pi/2 - \theta)} = -V_{xy}^0$, which exactly meets the experimental observation. In addition, Equations (3) and (6) explain the coincidence of longitudinal and transverse signals in Figure 3, because both are proportional to n_f. At $T \geq T_c^{mid}$, n_f decreases rapidly since the superconducting Cooper pairs dissociate. This explains the drop in V_{xy}^0 above T_c^{mid}. The nonzero V_{xy}^0 is extended to 26.0 K, suggesting superconducting phase fluctuations above T_c, such as the case in cuprate superconductors [20].

We also measured the transverse voltage under external magnetic fields. Figure 4a shows temperature dependence of V_{xy}^{H+} and V_{xy}^{H-} defined in the experimental paragraph. In the normal state above T_c^{onset}, V_{xy}^{H+} and V_{xy}^{H-} are mutually antisymmetric with respect to the applied field, consistent with usual Hall effect. The Hall voltage V_{xy}^{Hall}, obtained by $V_{xy}^{Hall} = (V_{xy}^{H+} - V_{xy}^{H-})/2$, is shown in Figure 4b. Indeed, V_{xy}^{Hall} increases linearly with increasing field in the normal state (shown in the inset). The value and sign of V_{xy}^{Hall} is consistent with previous reports [28]. At the superconducting transition, an anomalous sign reversal was observed, similar to previous study on Ba(Fe$_{0.9}$Co$_{0.1}$)$_2$As$_2$ crystal [43]. Here we emphasize that this anomalous sign reversal is related to applied fields, as it changes sign upon field reversal. Further discussion on its origin is beyond the scope of this paper.
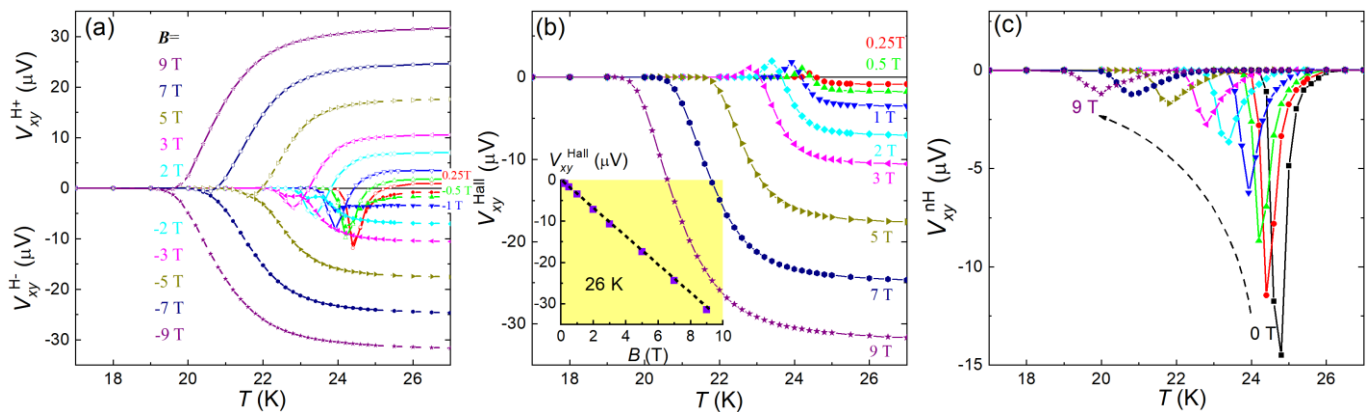
Figure 4. (**a**) Transverse voltages V_{xy}^{H+} and V_{xy}^{H-} at different directions of external magnetic fields as functions of temperature for the Ba(Fe$_{0.914}$Co$_{0.086}$)$_2$As$_2$ crystals. (**b**) and (**c**) plot the temperature dependence of Hall and non-Hall transverse voltages, respectively. See the experimental method in the text for details.

At the superconducting transition, however, the transverse voltage does not change sign upon reversal of magnetic field, especially under low magnetic fields. So, there exists a non-Hall-type signal V_{xy}^{nH}, which is shown in Figure 4c. Similar to the V_{xy}^0 signal shown in Figure 3, V_{xy}^{nH} also exhibits a peak at the superconducting transition, and the peak height decreases systematically with increasing magnetic field, which implies that V_{xy}^{nH}, together with V_{xy}^0, comes from the same origin. If V_{xy}^{nH} is due to the guided motion of vortices, as was earlier discussed in Na-Ta foils [42], the decrease in V_{xy}^{nH} can be qualitatively explained

by the decrease of anisotropic pinning under magnetic fields (the pinning force perpendicular to the vortex-guided direction is reduced by the increasing number of vortices (due to the increasing magnetic field), and the vortices may easily slip along this direction, which smears out the anisotropic pinning effect). Here we should mention an alternative explanation for the non-Hall voltages in terms of asymmetric inhomogeneity [44]. However, even if some unavoidable minor asymmetric inhomogeneity plays a role for the non-Hall signal, it cannot bring about the BKT dynamics with $\alpha(T) = 3$ at T_{BKT} by itself. Besides, numerical simulations [45] indicate that inhomogeneity in T_c merely broadens the BKT transition without changing the universality class ($z = 2$), which agrees with our experimental observations.

4. Summary and Discussion

The possible appearance of BKT-type phase transition in $Ba(Fe_{1-x}Co_x)_2As_2$ bulk crystals suggests a quasi-2D nature for iron-based superconductivity. Indeed, 2D antiferromagnetic spin fluctuations, which are mostly believed to be the glue of Cooper pairing, were revealed in $BaFe_{1.84}Co_{0.16}As_2$ by neutron scattering experiment [46]. The 2D nature of superfluid density was found in $Li(C_5H_5N)_{0.2}Fe_2Se_2$ superconductor [47]. Recently, a 2D-like (or BKT-like) nature in organic ion intercalated FeSe superconductors $(TBA)_xFeSe$ is also supported by both anisotropic transport and $I - V$ curves [48]. Furthermore, the observation of high-temperature superconductivity in FeSe monolayer grown on $SrTiO_3$ substrate [49] directly suggests 2D superconductivity in FeSCs. The thickness of the FeSe monolayer is only about 2.8 Å, which means that the coherence length perpendicular to the layers, ξ_c, is shorter than 2.8 Å. Therefore, it is not so surprising that 2D superconducting behavior was manifested in $Ba(Fe_{1-x}Co_x)_2As_2$, because the FeAs interlayer spacing is about 6.5 Å [28]. Here we point out that the conventional estimation of ξ_c from the anisotropy ratio in H_{c2} [50] using $\xi_{ab}/\xi_c = H_{c2}^{//}/H_{c2}^{\perp}$, which gives $\xi_c \sim 25$ Å, may be misleading. This is because the measured H_{c2} values are basically Pauli-limited (rather than orbital-limited) and FeSC are multi-band superconductors. For a specific superconducting pairing channel, ξ_c could be significantly smaller than the simple estimated from H_{c2}.

To summarize, we have presented the possible evidence for BKT phase transition in a typical FeSC $Ba(Fe_{0.914}Co_{0.086})_2As_2$. The observation of non-Hall transverse voltage, probably caused by the guided motion of thermally activated vortices, in turn, further indicates the BKT scenario with vortex–antivortex unbinding. Our results suggest that, similarly to CuSCs, two-dimensionality also plays an important role for high-temperature superconductivity in iron pnictides.

References

1. Mazin, I.I. Superconductivity gets an iron boost. *Nature* **2010**, *464*, 183–186. [CrossRef]
2. Basov, D.N.; Chubukov Andrey, V. Manifesto for a higher T_c. *Nat. Phys.* **2011**, *7*, 272–276. [CrossRef]
3. Scalapino, D.J. A common thread: The pairing interaction for unconventional superconductors. *Rev. Mod. Phys.* **2012**, *84*, 1383–1417. [CrossRef]

4. Yuan, H.Q.; Singleton, J.; Balakirev, F.; Baily, S.A.; Chen, G.F.; Luo, J.L.; Wang, N.L. Nearly isotropic superconductivity in $(Ba,K)Fe_2As_2$. *Nature* **2009**, *457*, 565–568. [CrossRef] [PubMed]
5. Ni, N.; Bud'ko, S.L.; Kreyssig, A.; Nandi, S.; Rustan, G.E.; Goldman, A.I.; Gupta, S.; Corbett, J.D.; Kracher, A.; Canfield, P.C. Anisotropic thermodynamic and transport properties of single-crystalline $Ba_{1-x}K_xFe_2As_2$ (x = 0 and 0.45). *Phys. Rev. B* **2008**, *78*, 014507. [CrossRef]
6. Blatter, G.; Feigel'Man, M.V.; Geshkenbein, V.B.; Larkin, A.I.; Vinokur, V.M. Vortices in high-temperature superconductors. *Rev. Mod. Phys.* **1994**, *66*, 1125–1388. [CrossRef]
7. Anderson, P.W. *The Theory of Superconductivity in the High-T_c Cuprate Superconductivity*; Princeton University Press: Princeton, NJ, USA, 1997.
8. Kosterlitz, J.M.; Thouless, D.J. Ordering, metastability and phase transitions in two-dimensional systems. *J. Phys. C* **1973**, *6*, 1181. [CrossRef]
9. Martin, S.; Fiory, A.T.; Espinosa, G.P.; Cooper, A.S.; Fleming, R.M. Vortex-Pair Excitation near the Superconducting Transition of $Bi_2Sr_2CaCu_2O_8$ Crystals. *Phys. Rev. Lett.* **1989**, *62*, 677–680. [CrossRef] [PubMed]
10. Artemenko, S.; Gorlova, I.; Latyshev, Y. Vortex motion and kosterlitz-thouless transition in superconducting single crystals $Bi_2Sr_2CaCu_2O_x$. *Phys. Lett. A* **1989**, *138*, 428–434. [CrossRef]
11. Stamp, P.C.E.; Forro, L.; Ayache, C. Kosterlitz-Thouless transition of fluxless solitons in superconducting $YBa_2Cu_3O_{7-\delta}$ single crystals. *Phys. Rev. B* **1988**, *38*, 2847. [CrossRef]
12. Yeh, N.-C.; Tsuei, C.C. Quasi-two-dimensional phase fluctuations in bulk superconducting $YBa_2Cu_3O_7$ single crystals. *Phys. Rev. B* **1989**, *39*, 9708–9711. [CrossRef]
13. Li, Q.; Huecker, M.; Gu, G.D.; Tsvelik, A.M.; Tranquada, J.M. Two-Dimensional Superconducting Fluctuations in Stripe-Ordered $La_{1.875}Ba_{0.125}CuO_4$. *Phys. Rev. Lett.* **2007**, *99*, 067001. [CrossRef] [PubMed]
14. Beasley, M.R.; Mooij, J.E.; Orlando, T.P. Possibility of Vortex-Antivortex Pair Dissociation in Two-Dimensional Superconductors. *Phys. Rev. Lett.* **1979**, *42*, 1165–1168. [CrossRef]
15. Hebard, A.F.; Fiory, A.T. Evidence for the Kosterlitz-Thouless transition in thin superconducting aluminum films. *Phys. Rev. Lett.* **1980**, *44*, 291. [CrossRef]
16. Jensen, H.J.; Minnhagen, P. Two-dimensional vortex fluctuations in the nonlinear current-voltage characteristics for high-temperature superconductors. *Phys. Rev. Lett.* **1991**, *66*, 1630–1633. [CrossRef] [PubMed]
17. Bulaevskii, L.N.; Ledvij, M.; Kogan, V.G. Fluctuations of vortices in layered high-T_c superconductors. *Phys. Rev. Lett.* **1992**, *68*, 3773. [CrossRef]
18. Vasek, P. Transverse voltage in high-T_c superconductors in zero magnetic fields. *Phys. C Supercond.* **2001**, *364–365*, 194–196. [CrossRef]
19. Janeček, I.; Vašek, P. Reciprocity theorem in high-temperature superconductors. *Phys. C Supercond.* **2003**, *390*, 330–340. [CrossRef]
20. Xu, Z.A.; Ong, N.P.; Wang, Y.; Kakeshita, T.; Uchida, S.I. Vortex-like excitations and the onset of superconducting phase fluctuation in underdoped $La_{2-x}Sr_x CuO_4$. *Nature* **2000**, *406*, 486–488. [CrossRef]
21. Pallecchi, I.; Fanciulli, C.; Tropeano, M.; Palenzona, A.; Ferretti, M.; Malagoli, A.; Martinelli, A.; Sheikin, I.; Putti, M.; Ferdeghini, C. Upper critical field and fluctuation conductivity in the critical regime of doped SmFeAsO. *Phys. Rev. B* **2009**, *79*, 104515. [CrossRef]
22. Lee, H.-S.; Park, J.-H.; Lee, J.-Y.; Kim, J.-Y.; Sung, N.-H.; Cho, B.; Lee, H.-J. Two-dimensional superconductivity of $SmFeAsO_{0.85}$ single crystals: A fluctuation-conductivity study. *Phys. C Supercond.* **2010**, *470*, S422–S423. [CrossRef]
23. Rullier-Albenque, F.; Colson, D.; Forget, A.; Alloul, H. Multiorbital Effects on the Transport and the Superconducting Fluctuations in LiFeAs. *Phys. Rev. Lett.* **2012**, *109*, 187005. [CrossRef]
24. Fanfarillo, L.; Benfatto, L.; Caprara, S.; Castellani, C.; Grilli, M. Theory of fluctuation conductivity from interband pairing in pnictide superconductors. *Phys. Rev. B* **2009**, *79*, 172508. [CrossRef]
25. Ge, J.; Cao, S.; Yuan, S.; Kang, B.; Zhang, J. Three-dimensional superconductivity in nominal composition Fe1.03Se with up to 10.9 K induced by internal strain. *J. Appl. Phys.* **2010**, *108*, 53903. [CrossRef]
26. Marra, P.; Nigro, A.; Li, Z.; Chen, G.F.; Wang, N.L.; Luo, J.L.; Noce, C. Paraconductivity of the K-doped $SrFe_2As_2$ superconductor. *N. J. Phys.* **2012**, *14*, 043001. [CrossRef]
27. Tang, F.; Wang, P.; Wang, P.; Gan, Y.; Gu, G.D.; Zhang, W.; He, M.; Zhang, L. Quasi-2D superconductivity in $FeTe_{0.55}Se_{0.45}$ ultrathin film. *J. Phys. Condens. Matter* **2019**, *31*, 265702. [CrossRef]
28. Wang, X.F.; Wu, T.; Wu, G.; Liu, R.H.; Chen, H.; Xie, Y.L.; Chen, X.H. The peculiar physical properties and phase diagram of $BaFe_{2-x}Co_xAs_2$ single crystals. *N. J. Phys.* **2009**, *11*, 045003. [CrossRef]
29. Fisher, D.S.; Fisher, M.P.A.; Huse, D.A. Thermal fluctuations, quenched disorder, phase transitions, and transport in type-II superconductors. *Phys. Rev. B* **1991**, *43*, 130–159. [CrossRef]
30. Jiang, S.; Xing, H.; Xuan, G.; Ren, Z.; Wang, C.; Xu, Z.-A.; Cao, G. Superconductivity and local-moment magnetism in $Eu(Fe0_{.89}Co_{0.11})_2As_2$. *Phys. Rev. B* **2009**, *80*, 184514. [CrossRef]
31. Van der Pauw, L.J. A method of measuring specific resistivity and Hall effect of discs of arbitrary shape. *Philips Res. Rep.* **1958**, *13*, 1–9.
32. Sample, H.H.; Bruno, W.J.; Sample, S.B.; Sichel, E.K. Reverse-field reciprocity for conducting specimens in magnetic fields. *J. Appl. Phys.* **1987**, *61*, 1079–1084. [CrossRef]

33. Pierson, S.W.; Friesen, M.; Ammirata, S.M.; Hunnicutt, J.C.; Gorham, L.A. Dynamic scaling for two-dimensional superconductors, Josephson-junction arrays, and superfluids. *Phys. Rev. B* **1999**, *60*, 1309–1325. [CrossRef]

34. Halperin, B.I.; Nelson, D.R. Resistive transition in superconducting films. *J. Low Temp. Phys.* **1979**, *36*, 599–616. [CrossRef]

35. Aslamazov, L.G.; Larkin, A.I. Effect of fluctuations on the properties of a superconductor above the critical temperature. *Sov. Phys. Solid State* **1968**, *10*, 875. [CrossRef]

36. Tinkham, M. *Introduction to Superconductivity*, 2nd ed.; McGraw-Hill: New York, NY, USA, 1996.

37. Nelson, D.R.; Kosterlitz, J.M. Universal Jump in the Superfluid density of two-dimensional superfluids. *Phys. Rev. Lett.* **1977**, *39*, 1201–1205. [CrossRef]

38. Lv, J.-P.; Liu, H.; Chen, Q.-H. Phase transition in site-diluted Josephson junction arrays: A numerical study. *Phys. Rev. B* **2009**, *79*, 104512. [CrossRef]

39. Vašek, P.; Janeček, I.; Plecháček, V. Intrinsic pinning and guided motion of vortices in high-T_c superconductors. *Phys. C Supercond.* **1995**, *247*, 381–384. [CrossRef]

40. Chu, J.-H.; Analytis, J.G.; De Greve, K.; McMahon, P.L.; Islam, Z.; Yamamoto, Y.; Fisher, I.R. In-plane resistivity anisotropy in an underdoped iron arsenide superconductor. *Science* **2010**, *329*, 824–826. [CrossRef] [PubMed]

41. Yin, Y.; Zech, M.; Williams, T.L.; Wang, X.F.; Wu, G.; Chen, X.H.; Hoffman, J.E. Scanning tunneling spectroscopy and vortex imaging in the iron pnictide superconductor BaFe$_{1.8}$Co$_{0.2}$As$_2$. *Phys. Rev. Lett.* **2009**, *102*, 097002. [CrossRef] [PubMed]

42. Niessen, A.K.; Weijsenfeld, C.H. Anisotropic Pinning and Guided Motion of Vortices in Type-II Superconductors. *J. Appl. Phys.* **1969**, *40*, 384–393. [CrossRef]

43. Wang, L.M.; Sou, U.C.; Yang, H.C.; Chang, L.J.; Cheng, C.M.; Tsuei, K.D.; Su, Y.; Wolf, T.; Adelmann, P. Mixed-state Hall effect and flux pinning in Ba(Fe$_{1-x}$Co$_x$)$_2$As$_2$ single crystals (x = 0.08 and 0.10). *Phys. Rev. B* **2011**, *83*, 134506. [CrossRef]

44. Segal, A.; Karpovski, M.; Gerber, A. Inhomogeneity and transverse voltage in superconductors. *Phys. Rev. B* **2011**, *83*, 094531. [CrossRef]

45. Cotón, N.; Ramallo, M.; Vidal, F. Effects of critical temperature inhomogeneities on the voltage–current characteristics of a planar superconductor near the Berezinskii–Kosterlitz–Thouless transition. *Supercond. Sci. Technol.* **2011**, *24*, 085013. [CrossRef]

46. Lumsden, M.D.; Christianson, A.D.; Parshall, D.; Stone, M.B.; Nagler, S.E.; MacDougall, G.J.; Mook, H.A.; Lokshin, K.; Egami, T.; Abernathy, D.L.; et al. Two-dimensional resonant magnetic excitation in BaFe$_{1.84}$Co$_{0.16}$As$_2$. *Phys. Rev. Lett.* **2009**, *102*, 107005. [CrossRef]

47. Biswas, P.K.; Krzton-Maziopa, A.; Khasanov, R.; Luetkens, H.; Pomjakushina, E.; Conder, K.; Amato, A. Two-Dimensional Superfluid Density in an Alkali Metal-Organic Solvent Intercalated Iron Selenide Superconductor Li(C$_5$H$_5$N)$_{0.2}$Fe$_2$Se$_2$. *Phys. Rev. Lett.* **2013**, *110*, 137003. [CrossRef]

48. Kang, B.L.; Shi, M.Z.; Li, S.J.; Wang, H.H.; Zhang, Q.; Zhao, D.; Li, J.; Song, D.W.; Zheng, L.X.; Nie, L.P.; et al. Preformed cooper pairs in layered FeSe-based superconductors. *Phys. Rev. Lett.* **2020**, *125*, 097003. [CrossRef] [PubMed]

49. Wang, Q.-Y.; Li, Z.; Zhang, W.-H.; Zhang, Z.-C.; Zhang, J.-S.; Li, W.; Ding, H.; Ou, Y.-B.; Deng, P.; Chang, K.; et al. Interface-induced high-temperature superconductivity in single unit-cell FeSe films on SrTiO$_3$. *Chin. Phys. Lett.* **2012**, *29*, 037402. [CrossRef]

50. Kano, M.; Kohama, Y.; Graf, D.; Balakirev, F.; Sefat, A.S.; Mcguire, M.A.; Sales, B.C.; Mandrus, D.; Tozer, S.W. Anisotropy of the upper critical field in a Co-doped BaFe$_2$As$_2$ single crystal. *J. Phys. Soc. Jpn.* **2009**, *78*, 084719. [CrossRef]